Letter

Tunable meron pair excitations and Berezinskii-Kosterlitz-Thouless phase transitions in the monolayer antiferromagnet $MnPSe_3$

Guokai Liao [1], Shunhong Zhang [1,2,*], Ping Cui [1,2,†] and Zhenyu Zhang [1,2]

[1] *International Center for Quantum Design of Functional Materials (ICQD), University of Science and Technology of China, Hefei 230026, Anhui, China*

[2] *Hefei National Laboratory, University of Science and Technology of China, Hefei, Anhui 230088, China*

(Received 14 July 2023; accepted 21 February 2024; published 11 March 2024)

Exploration of exotic quantum physics in magnetic systems of reduced dimensionality is among the central themes of condensed matter physics. Here we investigate the nature of magnetic couplings, topological excitations, and critical phenomena in monolayer $MnPSe_3$, a representative two-dimensional antiferromagnet. We first establish, based on first-principles calculations, that the $S = 5/2$ Mn^{2+} ions possess single-ion anisotropy, favoring in-plane magnetization, and exhibit isotropic antiferromagnetic pairwise couplings. Next, our atomistic magnetics simulations identify antiferromagnetically coupled meron pairs to be the characteristic topological excitations, whose size, polarity, and dynamics can be delicately tuned by an external magnetic field. Significantly, a critical temperature of ∼30 K is indicated in both the susceptibility and specific heat, and detailed scaling analyses on the spin correlations and stiffness unambiguously attribute the critical behavior to the Berezinskii-Kosterlitz-Thouless universality class. Our findings thereby provide an ideal candidate antiferromagnetic counterpart of the recently identified monolayer XY ferromagnet of $CrCl_3$, the former may harbor distinct topological excitations and multicriticality.

DOI: 10.1103/PhysRevB.109.L100403

Introduction. The discovery of two-dimensional (2D) crystals [1] opens the era of exploring novel quantum physics and critical phenomena in solid-state systems under reduced dimensionality, wherein the effects of different types of fluctuations become crucial [2–4]. Among these developments, the rise of monolayer magnetic materials provides fertile platforms for investigation of quantum magnetism in genuine 2D spin lattices. In monolayer ferromagnets, the development of long-range order [5–8] vitally relies on anisotropy in easy-axis magnetization. It has been further recognized that, with easy in-plane magnetization, topological defects in the form of vortex-antivortex pairs can be excited, which is the microscopic foundation for the celebrated Berezinskii-Kosterlitz-Thouless (BKT) phase transition [9–12] beyond the Landau scenario. As counterparts, antiferromagnets have also been thinned to the monolayer regime, with the transition-metal phosphorus trichalcogenides of $TMPX_3$ (TM = Cr, Mn, Fe, Co, Ni, and X = S, Se) [13–16] as the most extensively explored class [17]. This family of layer materials shares the commonality of hosting intralayer antiferromagnetism, favoring either the Néel or zigzag phase within the honeycomb lattice. These systems may provide not only ideal platforms for probing 2D antiferromagnetic (AFM) criticality and dynamics under various external fields [14,18–20], but also innovative technology potentials rooted in their inherent fast responses and non-stray-field characteristics [21,22]. The AFM coupling usually induces strong magnetic frustration and fluctuation to the system, capable of exciting or stabilizing various topological quasiparticles such as AFM skyrmions, in the presence [23–25] or even absence [26,27] of Dzyaloshinskii-Moriya (DM) interaction [28–30].

As compelling examples of novel physical phenomena harbored in the layer $TMPX_3$ compounds, a line of exotic observations has been reported as the systems reduce their thickness towards the monolayer limit. In particular, some monolayer systems exhibit clear signature of suppressed long-range AFM order [15], and may thus serve as candidate arenas to exhibit BKT criticality. Here, the systems inherently possess internal sublattice degrees of freedom beyond their ferromagnetic (FM) counterparts [31–34], potentially enabling richer variety and greater tunability of the local topological excitations with external fields.

In this work, we perform a comprehensive multiscale simulation study of the nature of magnetic couplings, topological excitations, and critical phenomena in monolayer $MnPSe_3$, which has been experimentally realized [14]. Based on first-principles calculations, we establish that the $S = 5/2$ Mn^{2+} ions possess single-ion anisotropy, favoring in-plane magnetization, and exhibit isotropic antiferromagnetic pairwise couplings. Next, our detailed atomistic magnetics simulations allow us to identify antiferromagnetically coupled meron pairs to be the characteristic topological excitations, whose size, polarity, and dynamics can be delicately tuned by an external magnetic field. Significantly, a critical temperature of ∼30 K is indicated in both the susceptibility and specific heat, and detailed scaling analyses on the spin correlations and stiffness unambiguously attribute the critical behavior to the

*szhang2@ustc.edu.cn
†cuipg@ustc.edu.cn

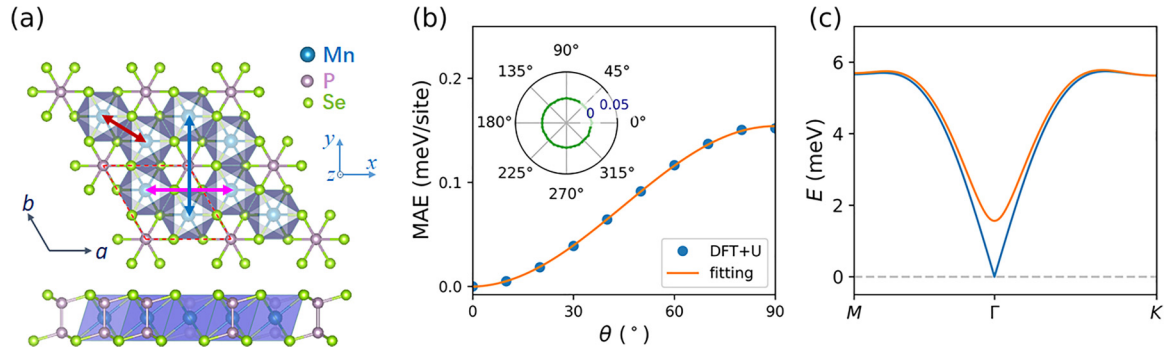

FIG. 1. (a) Top and side views of atomic structure of the $MnPSe_3$ monolayer. In the top view, the exemplified first, second, and third Mn-Mn pairs are respectively denoted by red, cyan, and blue dual-headed arrows. (b) MAE upon rotating the Néel vector of the AFM state from the in-plane (0°) to out-of-plane (90°) direction. The curve is a parabolic fitting using $\sin\theta$. The inset shows the MAE evolution (green circle) upon rotating the Néel vector within the xy plane. (c) The gapped and gapless spin excitation spectra calculated from an in-plane Néel configuration.

Berezinskii-Kosterlitz-Thouless universality class. Furthermore, by elevating the strength of the out-of-plane magnetic field, we can convert the AFM meron pairs into a new type of topological quasiparticles with FM-coupled core and AFM-coupled in-plane vorticity, with uncompensated topological charge. Collectively, our results provide valuable atomic-scale insights into the AFM-BKT physics harbored by the easy-plane $TMPX_3$ monolayers.

First-principles establishment of the spin Hamiltonian. Figure 1(a) schematically shows the crystal structure of monolayer $MnPSe_3$, composed of a honeycomb lattice formed by edge-sharing $MnSe_6$ octahedra and P dimers at the hollow sites. It is noted that recently monolayer $MnPSe_3$ has been experimentally synthesized, with its Néel vector and universality class demonstrated to be switchable to the Ising-type via in-plane strain [14]. We here focus on the equilibrium case subject to the XY regime, which has not yet been explicitly characterized in the monolayer limit.

We perform first-principles calculations [35] (see also Refs. [29,36–53] in the Supplemental Material) to obtain the equilibrium lattice structure and predominant exchange couplings of the $MnPSe_3$ monolayer. The rotationally invariant DFT+U approach [39] is applied to account for the strong onsite Coulomb repulsion of Mn-3d electrons, and spin-orbit coupling is included to resolve the magnetic anisotropy. The magnetic ground state within the collinear regime is verified to be Néel-type AFM, energetically more favorable than the FM, stripy-AFM, and zigzag-AFM phases by 66.0, 33.2, and 24.2 meV/Mn respectively, consistent with previous studies [54,55]. Figure 1(b) shows the magnetocrystalline anisotropy energy (MAE) upon rotating the Néel vector from in-plane to out-of-plane directions. The calculated MAE is 0.15 meV/Mn preferring in-plane magnetization, suggesting that the monolayer system is an intrinsic XY-like magnet.

Given the highly localized nature of Mn-3d electrons, the magnetic interactions within the $MnPSe_3$ monolayer can be described by a generic bilinear Hamiltonian

$$H = -\sum_i \mathbf{S}_i \mathbf{A}_i \mathbf{S}_i - \sum_{i<j} \mathbf{S}_i \mathbf{J}_{ij} \mathbf{S}_j \qquad (1)$$

where $\boldsymbol{S}_i$ is the spin operator of the ith Mn^{2+} ion with $|\mathbf{S}_i| = 5/2$, $\mathbf{A}_i$ and $\mathbf{J}_{ij}$ are 3×3 tensors quantifying the single-ion anisotropy (SIA) and two-ion exchange couplings up to the third-nearest-neighbor pairs, respectively. The threefold rotational symmetry reduces $\mathbf{A}_i$ to a scalar $A_i = A_{i,zz} - A_{i,xx}$, whose positive (negative) value favors out-of-plane (in-plane) magnetization. The inversion symmetry prohibits the existence of DM interactions [28,29] between the first- (1NN) and third-nearest-neighbor (3NN) pairs because the bisecting points of these pairs are located right at the inversion centers of the monolayer, while the second-nearest-neighbor (2NN) pair allow finite DMI with the DM vector perpendicular to the twofold rotation axis bisecting the bond, following Moriya's rule [29,30]. Other symmetry-allowed components of SIA and exchange couplings can be computed by using the well-developed four-state method [41–45]. By mapping the DFT+U total energies of a series of noncollinear magnetic configurations [46] to the spin Hamiltonian in Eq. (1), this approach enables a full anatomy of bilinear exchanges including non-Heisenberg terms that might influence the spin ground state or dynamics [56,57]. For the antisymmetric part of exchange couplings (DM interactions), the magnitude for the symmetry-allowed 2NN pairs is $|\mathbf{D}| = 8.28$ μeV, rather small and should have negligible effect on the spin dynamics; the 1NN and 3NN DM interactions are even smaller by one order of magnitude and can be viewed as numerical zero as required by symmetry (bond center at the inversion center of the monolayer). More details can be found in the Supplemental Material [35]. For the symmetric parts, all off-diagonal components of $\mathbf{J}_{ij}$ are calculated to be smaller than 1 μeV, while the diagonal components have strengths larger by several orders of magnitude (Table I), and are all AFM

TABLE I. Exchange couplings of the monolayer $MnPSe_3$ (in meV).

Exchange pair	J_{xx}	J_{yy}	J_{zz}
1NN	–0.582	–0.586	–0.586
2NN	–0.059	–0.058	–0.062
3NN	–0.332	–0.332	–0.332

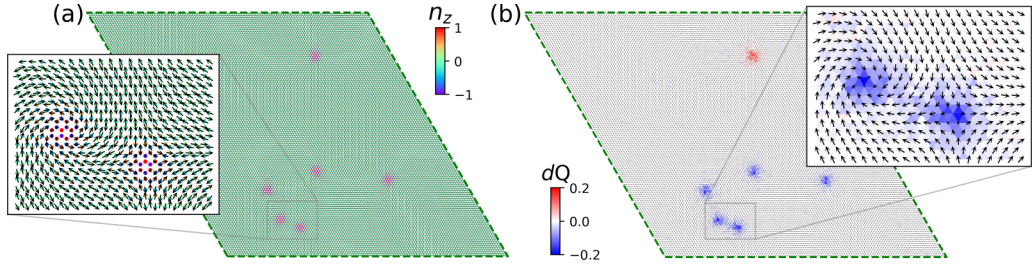

FIG. 2. Snapshots from an LLG simulation ($L = 120$) at 0.5 K, showing (a) magnetization of the antiferromagnetically coupled sublattices containing topological excitations, and (b) topological charge distribution on one sublattice. The insets are zoomed-in views of a meronic vortex/antivortex pair. The color coded n_z and dQ, respectively, represent the out-of-plane component of the spin vectors and the topological charge.

exhibiting negligible exchange anisotropy. Interestingly, the coupling strengths of the 2NN pairs are even smaller than those of 3NN, mainly due to the weaker hybridization with anion p orbitals on the corresponding superexchange paths, as has been elucidated based on collinear magnetic calculations [54]. The only nonvanishing SIA parameter is calculated to be $A_i = -0.035$ meV preferring in-plane magnetization, which accounts for the microscopic origin of MAE. As a running summary, our calculations characterize monolayer $MnPSe_3$ as an XY-type antiferromagnet, whose spin Hamiltonian can be effectively reduced to the form of an easy-plane SIA term plus AFM Heisenberg exchange couplings,

$$H = -\sum_i A_i S_{i,z}^2 - \sum_{i<j} J_{ij} \mathbf{S}_i \cdot \mathbf{S}_j. \tag{2}$$

Based on Eq. (2) parameterized as Table I, we can calculate the magnon spectrum of monolayer $MnPSe_3$ with an in-plane Néel ordered state, invoking the linear spin wave theory [58]. As presented in Fig. 1(c), the SIA lifts the degeneracy of the two branches, with the splitting more pronounced near the Γ point. The gapless lower mode indicates the absence of finite-temperature long-range order in monolayer $MnPSe_3$, consistent with 2D easy-plane anisotropy. In the language of symmetry breaking, this gapless magnon, with linear dispersion near the Γ point, signals the Goldstone mode associated with the broken U(1) symmetry. Such Goldstone mode is typically destructive to finite-temperature long-range order because it can introduce long-wavelength fluctuations to the system without energy cost.

BKT physics revealed by atomistic spin dynamics simulations. We now proceed to study the magnetic properties of monolayer $MnPSe_3$ based on the established spin Hamiltonian. The large magnetic moments of Mn^{2+} ions ($5\,\mu_B$) far away from the quantum limit can be treated eligibly as classical spins, and their dynamics are investigated by numerically integrating [52] the Landau-Lifshitz-Gilbert (LLG) equation [49,50] (see Supplemental Material, Note S1 [35] for details). The system, simulated by an $L \times L$ supercell, is cooled down from the paramagnetic state to various target temperatures and then equilibrated for subsequent analyses.

A representative snapshot, taken at $t = 30$ ps from a simulated cooling process lasting for 200 ps with $L = 120$, is shown in Fig. 2(a), revealing the emergence of antiferromagnetically coupled vortex/antivortex pairs. Indeed, such topological defects can be observed at the very beginning of the cooling process from a paramagnetic initial state ($t \sim 2$ ps), and all annihilate after $t > 125$ ps, leaving the system with zero topological charge while still presenting spin superfluidity behavior. Different from the archetypal 2D XY model [9,10] wherein spins near the vortex/antivortex cores have energetically unfavored large swirling angles, here the three-component spins of Heisenberg feature can accommodate out-of-plane vortex/antivortex cores, efficiently lowering the energy cost to excite topological defects [31]. In our simulations under fixed temperature of 0.5 K, the energy difference between a configuration containing 20 pairs of merons and another configuration with all merons annihilated is 0.223 meV/site. The topological charges of the emerging AFM vortices/antivortices can be calculated separately within the two sublattices [59] and should yield opposite values. As spatially resolved in Fig. 2(b) within one of the two sublattices, the topological charges peak at the core region of vortex/antivortex, and their integration over a single topological defect yields $-1/2$ (1/2), characterizing the excitations as merons (antimerons) commensurate with the in-plane magnetized background. A meron can be viewed as half a skyrmion, a more celebrated topological defect living in the out-of-plane magnetization background [60]. A pair of merons (insets of Fig. 2) restores the integer topological charge of ± 1, forming a bimeron. Being the characteristic topological excitations in BKT phase [61,62], merons in various systems can exhibit distinct dynamics and decaying rate. As ubiquitously seen in BKT systems, the vortexlike and antivortexlike meronic quasiparticles with opposite vorticity experience an attractive force, governing their motion towards each other and collapse even at low temperature. Consequently, the lifetime of vortex pairs in our simulated AFM system is typically no longer than 125 ps, as estimated by our topological charge analysis and statistics on consecutive snapshots extracted from atomistic spin dynamics simulations. The faster dynamics of AFM bimerons compared to their FM counterparts [63–65] is akin to skyrmionic systems [59].

Going beyond the real-space visualization of topological defects, we carry out systematic analysis of the thermodynamic properties in the spirit of ensemble average to gain further insights into the criticality of the AFM monolayer. Simulations are performed with a much longer time scale of $\sim 10^5$ ps at each target temperature to gather substantial equilibrium snapshot configurations for statistics. By varying the target temperature, we trace the evolution of thermodynamic observables including the normalized staggered

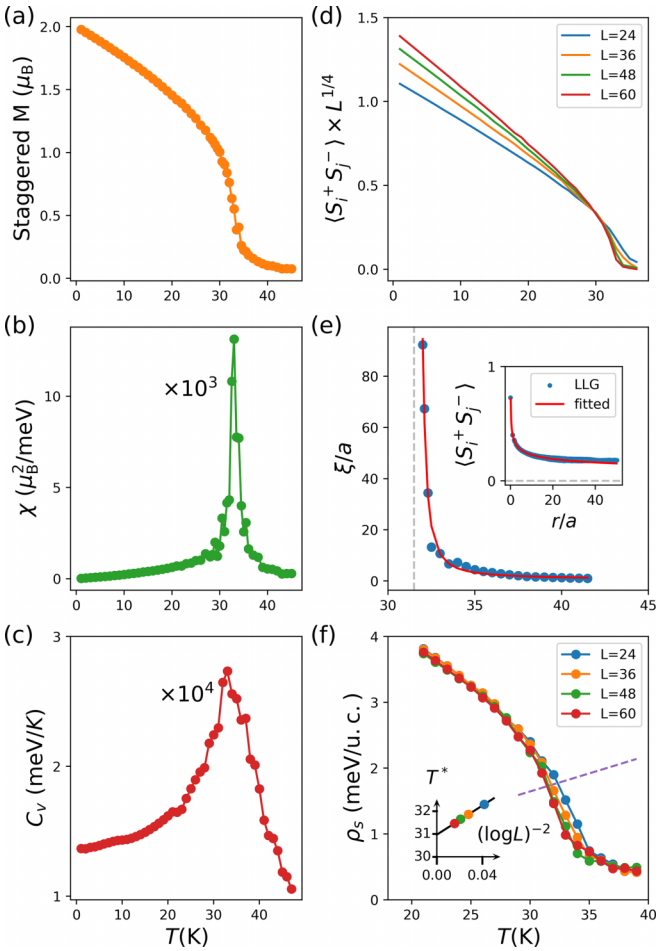

FIG. 3. Thermodynamic properties and scaling analyses of a monolayer $MnPSe_3$. Temperature dependence of (a) staggered magnetization, (b) susceptibility, and (c) specific heat obtained from LLG simulations ($L = 60$). (d) In-plane spin correlations between two most distant sites within the supercell, multiplied by $L^{1/4}$ for finite-size scaling analysis. (e) Correlation length as a function of temperature, fitted by Eq. (4). Inset: in-plane spin correlation at $T \sim 31.2$ K, fitted by the power-law decay $A(r/a)^{-1/4}$ (a being the lattice constant). (f) Spin stiffness as a function of temperature. For a given simulation size L, the crossing point between the corresponding curve and the purple dashed line defined by the BKT universality relation $\rho_s = 2k_B T/\pi$ yields a transition temperature $T^*(L)$. Inset: linear fitting using Eq. (5).

magnetization and its susceptibility, as well as the specific heat. As shown in Figs. 3(a)–3(c), these quantities coherently demonstrate that the system undergoes a magnetic transition at ~33 K. Due to easy-plane anisotropy, M_z is quenched to zero at all temperatures. The broad peak of susceptibility characterizes the 2D XY behavior, with a slowly decaying tail below the critical temperature distinct from the vanishing susceptibility commonly observed in prototypical Ising phase transitions.

It has long been established, based on renormalization group analysis [66] or quantum Monte Carlo simulations [67] in some simplified models with nearest-neighbor couplings, that even very weak easy-plane anisotropy can enable a Heisenberg spin system to present BKT criticality. However, for models associated with realistic materials, the interplay between multiple exchange couplings might mediate noncolinear long-range orders competing the BKT phase [68]. Even in the BKT regime, recent studies [69] elucidate that the involvements of long-range couplings can subtly alter the criticality. Analyses of the critical behavior based on the statistical results thus require extra caution. Typically, the T_{BKT} value estimated from specific heat and magnetic susceptibility may suffer from some quantitative uncertainty due to finite-size effect [70–72]. To access the true thermodynamic limit, reliably characterize BKT phase transition, and determine T_{BKT}, scaling analysis on the finite-size simulation results is necessary. Considering the in-plane spin components, for systems subject to the 2D XY universality class, the correlation function at $T = T_{BKT}$ satisfies

$$\langle S_i^+ S_j^- \rangle \sim L^{-1/4}, \tag{3}$$

with S_i and S_j being a pair of most distant spins within the supercell in size of L, and $S_i^{\pm} = S_i^x \pm \mathrm{i}S_i^y$. Given this scaling law, we can define a new scaling function $\langle S_i^+ S_j^- \rangle L^{1/4}$, which should predict the transition temperature independent of the supercell size. Figure 3(d) shows its temperature dependence, wherein the four curves corresponding to different L cross at the same transition temperature of 30.2 K, laying a slight correction on the value obtained from susceptibility and specific heat analyses.

Elevating the temperature across T_{BKT}, the spatial decay behavior of in-plane spin correlations switches from ¼ power law to exponential. At the critical temperature, the correlation length ξ diverges. This universal property provides an alternative way to confirm the BKT nature of the phase transition by fitting the high-temperature sector of the ξ-T curve, which satisfies

$$\xi \sim \exp\left[b(T - T_{BKT})^{-1/2}\right] \tag{4}$$

with b a system-specific parameter. Figure 3(e) shows such exponential fitting from which we attain $T_{BKT} \sim 31.2$ K in nice consistence with scaling analysis. As a crosscheck from the low-temperature side, our power-law fitting of the in-plane spin correlation at $T = 31.2$ K [inset of Fig. 3(e)] attests it as the lower bound of transition temperature.

From the viewpoint of energetics, another quantity eligible for scaling analysis is the spin stiffness ρ_s. As a temperature-dependent thermodynamic quantity, ρ_s measures the free energy cost to achieve an infinitesimal phase twist, or gradient, to the spin system, which can characterize the whirling energy of thermally excited topological defects. The spin stiffness is finite at the low-temperature BKT phase, and vanishes above the transition temperature; critically, at $T = T_{BKT}$, it follows a universal relationship, $\rho_s = 2k_B T/\pi$ [73]. In practice, the logarithmic finite-size correction to T_{BKT} has to be considered in the simulations, which reads [74]

$$T^*(L) = T_{BKT} + C(\ln L)^{-2}. \tag{5}$$

$T^*(L)$ is extracted from the crossing between the line representing the universal $\rho_s = 2k_B T/\pi$ relationship and the $\rho_s(T)$ curves from finite-size simulations, and C is a system-specific constant. Figure 3(f) presents such scaling analysis of ρ_s, from which we extrapolate the linearly fitted $T^*-(\ln L)^{-2}$ correlation to the thermodynamic limit and estimate that

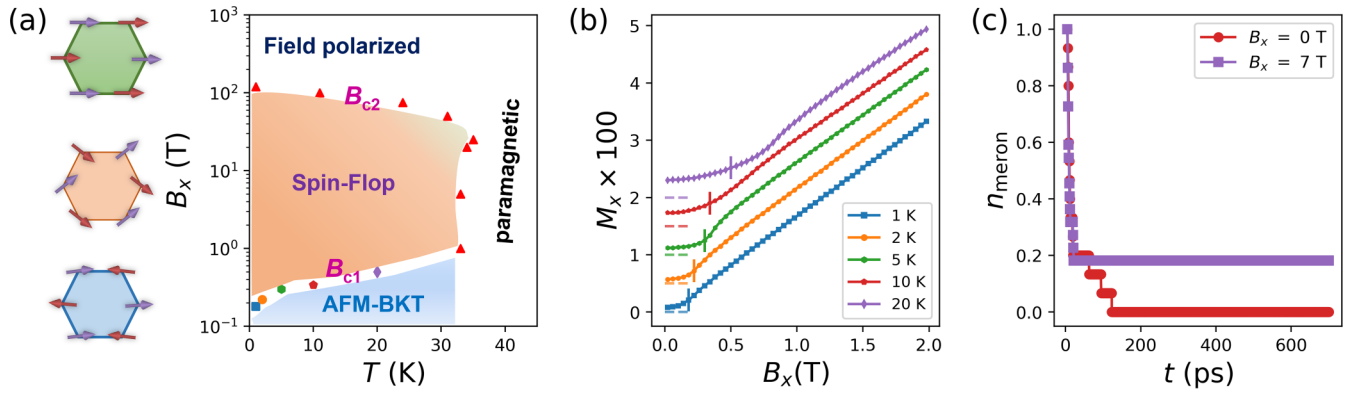

FIG. 4. (a) Schematic phase diagram of a monolayer $MnPSe_3$ under an in-plane magnetic field along x, B_x. Panels on the left sketch the corresponding short-range spin alignments in the identified phases color highlighted in the diagram. (b) Magnetization along x as a function of B_x and temperature. The curves are vertically shifted for clarity, with the zeros indicated by the corresponding horizontal dashed lines. The upturning points denoted by the vertical bars determine the temperature-dependent B_{c1} marked in (a). (c) Evolution of the normalized meron density upon cooling the system to $T = 0.5$ K without and with B_x.

$T_{BKT} \sim 31$ K, again in good accordance with previous analyses.

We have thus far confirmed intrinsic Néel-type AFM-BKT physics in monolayer $MnPSe_3$, the underlying mechanism of which can be understood via analyzing the interplay between exchange couplings, single-ion anisotropy, and lattice geometry. In the J_1-J_2-J_3-A model, All J_i's are isotropic and negative, but due to the honeycomb geometry, J_1 and J_3 favor intersublattice AFM coupling, while J_2 favors intrasublattice AFM coupling. The calculated J_1 and J_3 overwhelm J_2 in magnitude, thus the Néel correlation prevails in the honeycomb lattice, coupling the two sublattice antiferromagnetically. The SIA term A, which favors in-plane magnetization and is isotropic within the XY plane, constitutes the only interaction to induce magnetic anisotropy and drives the system to the AFM-BKT regime with quasi-long-range order and meronic excitations at low temperature.

Field-tunable phases and meron pairs. Unlike ferromagnets, AFM systems encompassing staggered magnetized sublattices respond to external magnetic fields in a macroscopically less sensitive manner. Microscopically, the competition between the Zeeman interaction and AFM exchange couplings can be regarded as magnetic frustration, which might mediate richer physics in topological excitations and vortex dynamics. For uniaxially anisotropic Heisenberg antiferromagnets, applying a uniform magnetic field along the easy axis can switch it from the long-range AFM order to the spin-flop (SF) phase [75–77], the latter featuring FM (AFM) alignment of magnetic moments along (perpendicular) to the easy axis. It would be intriguing to exploit relevant physics in BKT systems with quasi-long-range order and topological excitations.

Given the easy-plane anisotropy, we first tackle the case of applying an in-plane field along the x axis (B_x), which breaks the planar rotational symmetry of the Hamiltonian. By performing LLG simulations and tracking proper order parameters, we identify three distinct phases in addition to the trivial paramagnetic state. The corresponding short-range spin alignments and B_x-T phase diagram are illustrated in Fig. 4(a). The magnetization along x is invoked as the order parameter to trace the phase evolution. As shown in Fig. 4(b), the curves appear flat when B_x is small, and upturn after B_x exceeds a temperature-dependent critical field B_{c1}, signaling a field-induced transition from the AFM-BKT to SF phase, which persists up to the critical temperature (Fig. S1). Interestingly, the transition temperature from the AFM-BKT/SF phase to the paramagnetic state exhibits weak dependence on B_x [Figs. S2(a) and S2(b)]. Our scaling analyses on the squared staggered magnetization and spin stiffness coherently suggest that the BKT physics is fully suppressed at $B_x = 20$T, and the transition becomes Ising-type [Figs. S3(a) and S3(c)]. When B_x is further raised to surpass a temperature-dependent critical value of B_{c2}, the system enters a field-polarized phase [Fig. 4(a)], namely, all spins align with the field, and the staggered magnetization vanishes [Fig. S4(a)].

The topological defects provide a real-space signature to further distinguish the SF phase from the low-field AFM-BKT regime. Our simulations indicate that the meron excitation and dynamics below B_{c1} resemble the field-free case. On the contrary, in the SF phase under $B_x > B_{c1}$, the major spin components remain antiferromagnetically aligned, favoring two energetically degenerate directions perpendicular to the field ($\pm y$ in the present case). Such in-plane anisotropy leads to formation of multidomain configurations and domain-wall-enriched meron dynamics. At $B_x = 7$T, the meron pairs are bounded to the Bloch-line-shaped domain and exhibit Néel-type geometry [Fig. S6(a)]. Compared to the field-free case, these domain-wall merons possess a substantially decreased mobility, and accordingly elongated lifetime. Figure 4(c) contrasts the temporal evolution of meron density in the AFM-BKT and the spin-flop regimes. In the zero-field case, all merons collapse within 125 ps, while the applied field $B_x =$ 7T significantly increases the lifetime of a portion of merons pining to the domain walls up to 500 ps. Such enhanced topological stability and frozen meron dynamics implies the formation of a meron glass state [78], which is observed in our simulations when B_x is in the interval from 5–10 T, thereby could be verified by the recently developed imaging technique [79]. Further increasing B_x to 20 T leads to severe

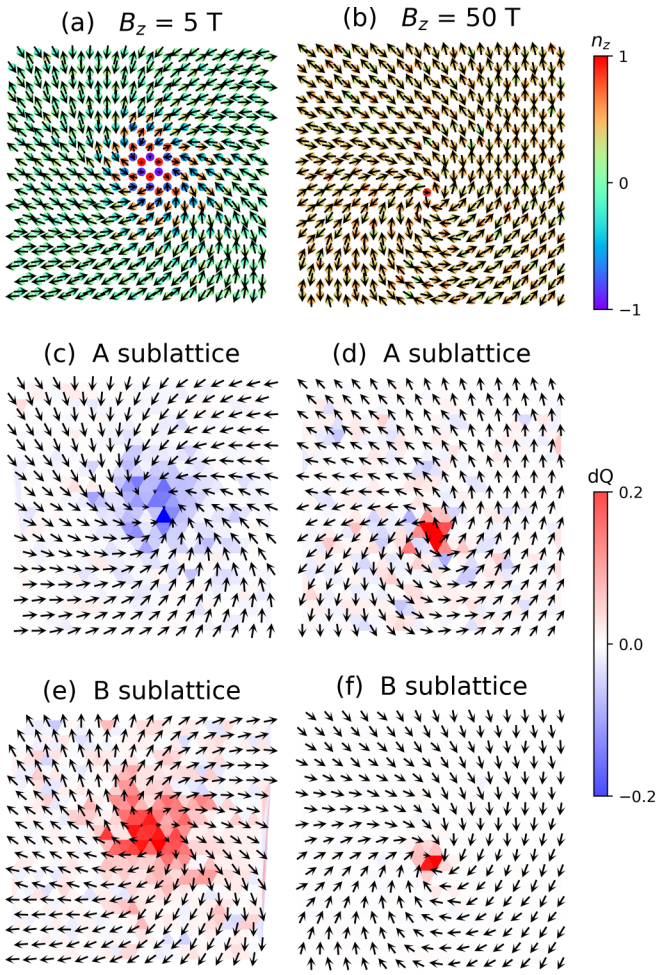

FIG. 5. Field-induced conversion of an AFM meron into a new type of FM-AFM hybrid meron. Snapshots from LLG simulations under an out-of-plane magnetic field (a), (c), (e) $B_z = 5$T and (b), (d), (f) $B_z = 50$T, corresponding to a typical AFM meron and a new FM-AFM hybrid meron, respectively. Color coding follows Fig. 2.

elongative distortion and eventual disappearance of the domain-wall merons [Fig. S6(b)].

Exertion of an out-of-plane magnetic field (B_z) induces a more laconic physics. Because the rotational symmetry of the Hamiltonian is preserved, the transition temperature and critical behavior in such B_z induced spin-flop phase [Figs. S2(c) and S2(d); Figs. S3(b) and S3(d)] do not exhibit obvious difference from the field-free case. The in-plane staggered magnetization is gradually suppressed when B_z is increased, before vanishing to zero at $B_z \sim 120$ T [Fig. S4(b)]. Figure S5 presents the phase diagram in the presence of B_z, illustrating the AFM phase falls into the spin-flop phase with arbitrary small B_z. Microscopically, the topological excitations in this circumstance are still merons presenting pairing behavior, but with shrinking core upon increasing B_z (Figs. S7 and S8). More importantly, a substantially large B_z can flip the out-of-plane polarizations of the meron cores within the two sublattices, from opposite [Fig. 5(a)] to aligned [Fig. 5(b)]; meanwhile, the in-plane whirling pattern remains intact albeit with smaller components under high field. Consequently, a drastic change to the topological charge distribution is induced as compared to the low-field case [Figs. 5(c), 5(e) vs. 5(d), 5(f)]. The vortices in such spin-flop BKT phase, with field-modulated polarization and uncompensated topological charge, can be viewed as an intermediate regime between the pure AFM-BKT phase discussed above and the well-studied FM-BKT systems [31–34]. It would be intriguing to explore possible additional criticality associated with the meron core flipping, which is the subject of future works.

Discussion and summary. Since its conceptualization, the BKT phase transition as a profound framework to unify abundant critical phenomena by topology has been observed in a plethora of condensed matters in two dimensions, including superfluid [80], superconducting [81], and ultracold atom systems [82]. For decades, efforts to realize BKT transitions in magnetic systems have mainly focused on quasi-2D layer XY-type magnets [83–90], wherein the unavoidable interlayer couplings may mediate 3D long-range magnetic order that competes or even suppresses the BKT phase. The topological excitations revealed here in monolayer $MnPSe_3$ suggest it as a promising candidate to probe magnetic BKT criticality and study the field-tunable AFM vortex dynamics. Exempted from the complexity of interlayer coupling encountered in multilayer magnets [83–90], characterization of the intrinsic BKT order in monolayer systems are likely more transparent and definitive [31–34]. Here we note that, given the ultrathin nature of monolayer antiferromagnets, neutron scattering or nuclear magnetic resonance widely utilized for detecting BKT physics in multilayer magnets [87–89] might become inapplicable. Promising approaches for verifying the AFM-BKT criticality and visualizing the topological excitations may include the polarized Raman spectroscopy [15] and some real-space imaging techniques [14,16,79].

Summarizing, our work provides a comprehensive characterization of the anisotropic magnetic interactions, the type and dynamics of the AFM topological excitations, and tunability of the criticality in the monolayer $MnPSe_3$. The insights from the present study can have broader implications beyond characterizing an intrinsic AFM-BKT order. The established phase diagram, the vortex dynamics harnessed by sub-Tesla B_x, and the newly identified meronic quasiparticles with flipped cores under B_z, collectively highlight the delicate interplay between the magnetic field and AFM coupling. Prospectively, it would also be intriguing to investigate how these fundamentally important responses evolve when chiral Dzyaloshinskii-Moriya interactions [91] are further introduced via proper symmetry reduction [92].

ACKNOWLEDGMENTS

We acknowledge Professor Wei Qin and Dr. Xiaoyin Li for helpful discussions and valuable suggestions. This work was supported by National Natural Science Foundation of China (Grants No. 11904350, No. 12374458, and No. 11974323), the Anhui Provincial Natural Science Foundation (Grant. No. 2008085QA30), the Innovation Program for Quantum Science and Technology (Grant No. 2021ZD0302800), the Strategic Priority Research Program of Chinese Academy of Sciences (Grant No. XDB0510200), and the Anhui Initiative in Quantum Information Technologies (Grant No. AHY170000).

[1] K. S. Novoselov, D. Jiang, F. Schedin, T. J. Booth, V. V. Khotkevich, S. V. Morozov, and A. K. Geim, Two-dimensional atomic crystals, Proc. Natl. Acad. Sci. **102**, 10451 (2005).

[2] P. C. Hohenberg, Existence of long-range order in one and two dimensions, Phys. Rev. **158**, 383 (1967).

[3] N. D. Mermin and H. Wagner, Absence of ferromagnetism or antiferromagnetism in one- or two-dimensional isotropic heisenberg models, Phys. Rev. Lett. **17**, 1133 (1966).

[4] H. E. Stanley, Dependence of critical properties on dimensionality of spins, Phys. Rev. Lett. **20**, 589 (1968).

[5] B. Huang, G. Clark, E. Navarro-Moratalla, D. R. Klein, R. Cheng, K. L. Seyler, D. Zhong, E. Schmidgall, M. A. McGuire, D. H. Cobden *et al.*, Layer-dependent ferromagnetism in a van der Waals crystal down to the monolayer limit, Nature (London) **546**, 270 (2017).

[6] C. Gong, L. Li, Z. Li, H. Ji, A. Stern, Y. Xia, T. Cao, W. Bao, C. Wang, Y. Wang *et al.*, Discovery of intrinsic ferromagnetism in two-dimensional van der Waals crystals, Nature (London) **546**, 265 (2017).

[7] Y. Deng, Y. Yu, Y. Song, J. Zhang, N. Z. Wang, Z. Sun, Y. Yi, Y. Z. Wu, S. Wu, J. Zhu *et al.*, Gate-tunable room-temperature ferromagnetism in two-dimensional Fe_3GeTe_2, Nature (London) **563**, 94 (2018).

[8] Z. Fei, B. Huang, P. Malinowski, W. Wang, T. Song, J. Sanchez, W. Yao, D. Xiao, X. Zhu, A. F. May *et al.*, Two-dimensional itinerant ferromagnetism in atomically thin Fe_3GeTe_2, Nat. Mater. **17**, 778 (2018).

[9] J. M. Kosterlitz and D. J. Thouless, Long range order and metastability in two dimensional solids and superfluids. (Application of dislocation theory), J. Phys. C: Solid State Phys. **5**, L124 (1972).

[10] J. M. Kosterlitz and D. J. Thouless, Ordering, metastability and phase transitions in two-dimensional systems, J. Phys. C: Solid State Phys. **6**, 1181 (1973).

[11] V. L. Berezinskii, Destruction of long-range order in one-dimensional and two-dimensional systems having a continuous symmetry group I. Classical systems, Zh. Eksp. Teor. Fiz. **59**, 907 (1971) [Sov. J. Expt. Theo. Phys. **32**, 493 (1971)].

[12] V. L. Berezinskii, Destruction of long-range order in one-dimensional and two-dimensional systems possessing a continuous symmetry group. II. Quantum systems, Zh. Eksp. Teor. Fiz. **61**, 1144 (1972) [Sov. J. Expt. Theo. Phys. **34**, 610 (1972)].

[13] J.-U. Lee, S. Lee, J. H. Ryoo, S. Kang, T. Y. Kim, P. Kim, C.-H. Park, J.-G. Park, and H. Cheong, Ising-type magnetic ordering in atomically thin $FePS_3$, Nano Lett. **16**, 7433 (2016).

[14] Z. Ni, A. V. Haglund, H. Wang, B. Xu, C. Bernhard, D. G. Mandrus, X. Qian, E. J. Mele, C. L. Kane, and L. Wu, Imaging the Néel vector switching in the monolayer antiferromagnet $MnPSe_3$ with strain-controlled Ising order, Nat. Nanotechnol. **16**, 782 (2021).

[15] K. Kim, S. Y. Lim, J.-U. Lee, S. Lee, T. Y. Kim, K. Park, G. S. Jeon, C.-H. Park, J.-G. Park, and H. Cheong, Suppression of magnetic ordering in XXZ-type antiferromagnetic monolayer $NiPS_3$, Nat. Commun. **10**, 345 (2019).

[16] Z. Ni, H. Zhang, D. A. Hopper, A. V. Haglund, N. Huang, D. Jariwala, L. C. Bassett, D. G. Mandrus, E. J. Mele, C. L. Kane *et al.*, Direct imaging of antiferromagnetic domains and anomalous layer-dependent mirror symmetry breaking in atomically thin $MnPS_3$, Phys. Rev. Lett. **127**, 187201 (2021).

[17] F. Wang, T. A. Shifa, P. Yu, P. He, Y. Liu, F. Wang, Z. Wang, X. Zhan, X. Lou, F. Xia *et al.*, New frontiers on van der Waals layered metal phosphorous trichalcogenides, Adv. Funct. Mater. **28**, 1802151 (2018).

[18] G. Long, H. Henck, M. Gibertini, D. Dumcenco, Z. Wang, T. Taniguchi, K. Watanabe, E. Giannini, and A. F. Morpurgo, Persistence of magnetism in atomically thin $MnPS_3$ crystals, Nano Lett. **20**, 2452 (2020).

[19] N. Sivadas, S. Okamoto, and D. Xiao, Gate-Controllable magneto-optic Kerr effect in layered collinear antiferromagnets, Phys. Rev. Lett. **117**, 267203 (2016).

[20] D. Afanasiev, J. R. Hortensius, M. Matthiesen, S. Mañas-Valero, M. Šiškins, M. Lee, E. Lesne, H. S. J. van der Zant, P. G. Steeneken, B. A. Ivanov *et al.*, Controlling the anisotropy of a van der Waals antiferromagnet with light, Sci. Adv. **7**, eabf3096 (2021).

[21] T. Jungwirth, X. Marti, P. Wadley, and J. Wunderlich, Antiferromagnetic spintronics, Nat. Nanotechnol. **11**, 231 (2016).

[22] V. Baltz, A. Manchon, M. Tsoi, T. Moriyama, T. Ono, and Y. Tserkovnyak, Antiferromagnetic spintronics, Rev. Mod. Phys. **90**, 015005 (2018).

[23] H. D. Rosales, D. C. Cabra, and P. Pujol, Three-sublattice skyrmion crystal in the antiferromagnetic triangular lattice, Phys. Rev. B **92**, 214439 (2015).

[24] X. Zhang, Y. Zhou, and M. Ezawa, Antiferromagnetic skyrmion: Stability, creation and manipulation, Sci. Rep. **6**, 24795 (2016).

[25] M. Mohylna and M. Žukovič, Stability of skyrmion crystal phase in antiferromagnetic triangular lattice with DMI and single-ion anisotropy, J. Magn. Magn. Mater. **546**, 168840 (2022).

[26] M. Mohylna, F. A. Gómez Albarracín, M. Žukovič, and H. D. Rosales, Spontaneous antiferromagnetic skyrmion/antiskyrmion lattice and spiral spin-liquid states in the frustrated triangular lattice, Phys. Rev. B **106**, 224406 (2022).

[27] S. Gao, H. D. Rosales, F. A. Gómez Albarracín, V. Tsurkan, G. Kaur, T. Fennell, P. Steffens, M. Boehm, P. Čermák, A. Schneidewind *et al.*, Fractional antiferromagnetic skyrmion lattice induced by anisotropic couplings, Nature (London) **586**, 37 (2020).

[28] I. Dzyaloshinsky, A thermodynamic theory of "weak" ferromagnetism of antiferromagnetics, J. Phys. Chem. Solids **4**, 241 (1958).

[29] T. Moriya, Anisotropic superexchange interaction and weak ferromagnetism, Phys. Rev. **120**, 91 (1960).

[30] T. Moriya, New mechanism of anisotropic superexchange interaction, Phys. Rev. Lett. **4**, 228 (1960).

[31] X. Lu, R. Fei, L. Zhu, and L. Yang, Meron-like topological spin defects in monolayer $CrCl_3$, Nat. Commun. **11**, 4724 (2020).

[32] M. Augustin, S. Jenkins, R. F. L. Evans, K. S. Novoselov, and E. J. G. Santos, Properties and dynamics of meron topological spin textures in the two-dimensional magnet $CrCl_3$, Nat. Commun. **12**, 185 (2021).

[33] M. Dupont, Y. O. Kvashnin, M. Shiranzaei, J. Fransson, N. Laflorencie, and A. Kantian, Monolayer $CrCl_3$ as an ideal test bed for the universality classes of 2D magnetism, Phys. Rev. Lett. **127**, 037204 (2021).

[34] A. Bedoya-Pinto, J.-R. Ji, A. K. Pandeya, P. Gargiani, M. Valvidares, P. Sessi, J. M. Taylor, F. Radu, K. Chang, and

S. S. P. Parkin, Intrinsic 2D-XY ferromagnetism in a van der Waals monolayer, Science **374**, 616 (2021).

[35] See Supplemental Material at http://link.aps.org/supplemental/10.1103/PhysRevB.109.L100403 for computational details, additional simulation results and analyses on the field tunable phases, and associated meron excitations and dynamics.

[36] G. Kresse and J. Furthmüller, Efficient iterative schemes for ab initio total-energy calculations using a plane-wave basis set, Phys. Rev. B **54**, 11169 (1996).

[37] P. E. Blöchl, Projector augmented-wave method, Phys. Rev. B **50**, 17953 (1994).

[38] J. P. Perdew, K. Burke, and M. Ernzerhof, Generalized gradient approximation made simple, Phys. Rev. Lett. **77**, 3865 (1996).

[39] S. L. Dudarev, G. A. Botton, S. Y. Savrasov, C. J. Humphreys, and A. P. Sutton, Electron-energy-loss spectra and the structural stability of nickel oxide: An LSDA+U study, Phys. Rev. B **57**, 1505 (1998).

[40] A. Wiedenmann, J. Rossat-Mignod, A. Louisy, R. Brec, and J. Rouxel, Neutron diffraction study of the layered compounds $MnPSe_3$ and $FePSe_3$, Solid State Commun. **40**, 1067 (1981).

[41] H. J. Xiang, E. J. Kan, S.-H. Wei, M. H. Whangbo, and X. G. Gong, Predicting the spin-lattice order of frustrated systems from first principles, Phys. Rev. B **84**, 224429 (2011).

[42] H. Xiang, C. Lee, H.-J. Koo, X. Gong, and M.-H. Whangbo, Magnetic properties and energy-mapping analysis, Dalton. Trans. **42**, 823 (2013).

[43] C. Xu, J. Feng, M. Kawamura, Y. Yamaji, Y. Nahas, S. Prokhorenko, Y. Qi, H. Xiang, and L. Bellaiche, Possible kitaev quantum spin liquid state in 2D materials with S = 3/2, Phys. Rev. Lett. **124**, 087205 (2020).

[44] D. Šabani, C. Bacaksiz, and M. V. Milošević, Ab initio methodology for magnetic exchange parameters: Generic four-state energy mapping onto a Heisenberg spin Hamiltonian, Phys. Rev. B **102**, 014457 (2020).

[45] D. Amoroso, P. Barone, and S. Picozzi, Spontaneous skyrmionic lattice from anisotropic symmetric exchange in a Ni-halide monolayer, Nat. Commun. **11**, 5784 (2020).

[46] P.-W. Ma and S. L. Dudarev, Constrained density functional for noncollinear magnetism, Phys. Rev. B **91**, 054420 (2015).

[47] C. Xu, J. Feng, S. Prokhorenko, Y. Nahas, H. Xiang, and L. Bellaiche, Topological spin texture in Janus monolayers of the chromium trihalides $Cr(I, X)_3$, Phys. Rev. B **101**, 060404(R) (2020).

[48] F. Zhu, L. Zhang, X. Wang, F. J. dos Santos, J. Song, T. Mueller, K. Schmalzl, W. F. Schmidt, A. Ivanov, J. T. Park *et al.*, Topological magnon insulators in two-dimensional van der Waals ferromagnets $CrSiTe_3$ and $CrGeTe_3$: Toward intrinsic gap-tunability, Sci. Adv. **7**, eabi7532 (2021).

[49] G. P. Müller, M. Hoffmann, C. Dißelkamp, D. Schürhoff, S. Mavros, M. Sallermann, N. S. Kiselev, H. Jónsson, and S. Blügel, Spirit: Multifunctional framework for atomistic spin simulations, Phys. Rev. B **99**, 224414 (2019).

[50] T. L. Gilbert, A phenomenological theory of damping in ferromagnetic materials, IEEE Trans. Magn. **40**, 3443 (2004).

[51] O. Chubykalo, J. D. Hannay, M. Wongsam, R. W. Chantrell, and J. M. Gonzalez, Langevin dynamic simulation of spin waves in a micromagnetic model, Phys. Rev. B **65**, 184428 (2002).

[52] P. Depondt and F. G. Mertens, Spin dynamics simulations of two-dimensional clusters with Heisenberg and dipole–dipole interactions, J. Phys. Condens. Matter **21**, 336005 (2009).

[53] B. Berg and M. Lüscher, Definition and statistical distributions of a topological number in the lattice $O(3)$ σ-model, Nucl. Phys. B. **190**, 412 (1981).

[54] N. Sivadas, M. W. Daniels, R. H. Swendsen, S. Okamoto, and D. Xiao, Magnetic ground state of semiconducting transition-metal trichalcogenide monolayers, Phys. Rev. B **91**, 235425 (2015).

[55] X. Li, X. Wu, and J. Yang, Half-Metallicity in $MnPSe_3$ exfoliated nanosheet with carrier doping, J. Am. Chem. Soc. **136**, 11065 (2014).

[56] C. Xu, J. Feng, H. Xiang, and L. Bellaiche, Interplay between Kitaev interaction and single ion anisotropy in ferromagnetic CrI_3 and $CrGeTe_3$ monolayers, Npj Comput. Mater. **4**, 57 (2018).

[57] I. Lee, F. G. Utermohlen, D. Weber, K. Hwang, C. Zhang, J. van Tol, J. E. Goldberger, N. Trivedi, and P. C. Hammel, Fundamental spin interactions underlying the magnetic anisotropy in the kitaev ferromagnet CrI_3, Phys. Rev. Lett. **124**, 017201 (2020).

[58] S. Toth and B. Lake, Linear spin wave theory for single-Q incommensurate magnetic structures, J. Phys. Condens. Matter **27**, 166002 (2015).

[59] J. Barker and O. A. Tretiakov, Static and dynamical properties of antiferromagnetic skyrmions in the presence of applied current and temperature, Phys. Rev. Lett. **116**, 147203 (2016).

[60] Y. Tokura and N. Kanazawa, Magnetic skyrmion materials, Chem. Rev. **121**, 2857 (2021).

[61] E. Schwartz, H. Vakili, M. Ali, and A. A. Kovalev, Spin Hall effect of vorticity, Phys. Rev. B **106**, L220401 (2022).

[62] S. K. Kim and S. B. Chung, Transport signature of the magnetic Berezinskii-Kosterlitz-Thouless transition, SciPost Physics **10**, 068 (2021).

[63] A. R. Völkel, F. G. Mertens, A. R. Bishop, and G. M. Wysin, Motion of vortex pairs in the ferromagnetic and antiferromagnetic anisotropic Heisenberg model, Phys. Rev. B **43**, 5992 (1991).

[64] A. R. Pereira and A. S. T. Pires, Dynamics of vortices in a two-dimensional easy-plane antiferromagnet, Phys. Rev. B **51**, 996 (1995).

[65] D. A. Dimitrov and G. M. Wysin, Free vortex and vortex-pair lifetimes in classical two-dimensional easy-plane magnets, J. Phys. Condens. Matter **10**, 7453 (1998).

[66] V. Y. Irkhin and A. A. Katanin, Kosterlitz-Thouless and magnetic transition temperatures in layered magnets with a weak easy-plane anisotropy, Phys. Rev. B **60**, 2990 (1999).

[67] A. Cuccoli, T. Roscilde, V. Tognetti, R. Vaia, and P. Verrucchi, Quantum Monte Carlo study of $S = 1/2$ weakly anisotropic antiferromagnets on the square lattice, Phys. Rev. B **67**, 104414 (2003).

[68] Y. Watanabe, S. Trebst, and C. Hickey, arXiv:2212.14053.

[69] G. Giachetti, N. Defenu, S. Ruffo, and A. Trombettoni, Berezinskii-Kosterlitz-Thouless phase transitions with long-range couplings, Phys. Rev. Lett. **127**, 156801 (2021).

[70] Y. Miyajima, Y. Murata, Y. Tanaka, and M. Mochizuki, Machine learning detection of Berezinskii-Kosterlitz-Thouless

transitions in q-state clock models, Phys. Rev. B **104**, 075114 (2021).

[71] T. Olsen, Theory and simulations of critical temperatures in CrI_3 and other 2D materials: Easy-axis magnetic order and easy-plane Kosterlitz-Thouless transitions, MRS Commun. **9**, 1142 (2019).

[72] S. Jenkins, L. Rózsa, U. Atxitia, R. F. L. Evans, K. S. Novoselov, and E. J. G. Santos, Breaking through the mermin-wagner limit in 2D van der Waals magnets, Nat. Commun. **13**, 6917 (2022).

[73] D. R. Nelson and J. M. Kosterlitz, Universal jump in the superfluid density of two-dimensional superfluids, Phys. Rev. Lett. **39**, 1201 (1977).

[74] S. T. Bramwell and P. C. W. Holdsworth, Magnetization and universal sub-critical behaviour in two-dimensional XY magnets, J. Phys. Condens. Matter **5**, L53 (1993).

[75] M. Holtschneider and W. Selke, Uniaxially anisotropic antiferromagnets in a field on a square lattice, Eur. Phys. J. B **62**, 147 (2008).

[76] R. Basnet, A. Wegner, K. Pandey, S. Storment, and J. Hu, Highly sensitive spin-flop transition in antiferromagnetic van der Waals material MPS_3 (M = Ni and Mn), Phys. Rev. Mater. **5**, 064413 (2021).

[77] F. B. Anderson and H. B. Callen, Statistical mechanics and field-induced phase transitions of the Heisenberg antiferromagnet, Phys. Rev. **136**, A1068 (1964).

[78] H. D. Rosales, F. A. G. Albarracín, P. Pujol, and L. D. C. Jaubert, Skyrmion fluid and bimeron glass protected by a chiral spin liquid on a kagome lattice, Phys. Rev. Lett. **130**, 106703 (2023).

[79] Y. Togawa, T. Akashi, H. Kasai, G. W. Paterson, S. McVitie, Y. Kousaka, H. Shinada, J.-I. Kishine, and J. Akimitsu, Formations of narrow stripes and vortex–antivortex pairs in a quasi-two-dimensional ferromagnet K_2CuF_4, J. Phys. Soc. Jpn. **90**, 014702 (2020).

[80] D. J. Bishop and J. D. Reppy, Study of the superfluid transition in two-dimensional ^{4}He films, Phys. Rev. Lett. **40**, 1727 (1978).

[81] D. J. Resnick, J. C. Garland, J. T. Boyd, S. Shoemaker, and R. S. Newrock, Kosterlitz-Thouless transition in proximity-coupled superconducting arrays, Phys. Rev. Lett. **47**, 1542 (1981).

[82] Z. Hadzibabic, P. Krüger, M. Cheneau, B. Battelier, and J. Dalibard, Berezinskii–Kosterlitz–Thouless crossover in a trapped atomic gas, Nature (London) **441**, 1118 (2006).

[83] L. P. Regnault, J. Rossat-Mignod, J. Y. Henry, and L. J. de Jongh, Magnetic properties of the quasi-2D easy plane antiferromagnet $BaNi_2(PO_4)_2$, J. Magn. Magn. Mater. **31–34**, 1205 (1983).

[84] P. Gaveau, J. P. Boucher, L. P. Regnault, and Y. Henry, Magnetic-field dependence of the phosphorus nuclear spin-relaxation rate in the quasi-two-dimensional XY antiferromagnet $BaNi_2(PO_4)_2$, J. Appl. Phys. **69**, 6228 (1991).

[85] M. Heinrich, H. A. Krug von Nidda, A. Loidl, N. Rogado, and R. J. Cava, Potential signature of a Kosterlitz-Thouless transition in $BaNi_2V_2O_8$, Phys. Rev. Lett. **91**, 137601 (2003).

[86] U. Tutsch, B. Wolf, S. Wessel, L. Postulka, Y. Tsui, H. O. Jeschke, I. Opahle, T. Saha-Dasgupta, R. Valentí, A. Brühl *et al.*, Evidence of a field-induced Berezinskii–Kosterlitz–Thouless scenario in a two-dimensional spin–dimer system, Nat. Commun. **5**, 5169 (2014).

[87] H. Li, Y. D. Liao, B.-B. Chen, X.-T. Zeng, X.-L. Sheng, Y. Qi, Z. Y. Meng, and W. Li, Kosterlitz-Thouless melting of magnetic order in the triangular quantum Ising material $TmMgGaO_4$, Nat. Commun. **11**, 1111 (2020).

[88] Z. Hu, Z. Ma, Y.-D. Liao, H. Li, C. Ma, Y. Cui, Y. Shangguan, Z. Huang, Y. Qi, W. Li *et al.*, Evidence of the Berezinskii-Kosterlitz-Thouless phase in a frustrated magnet, Nat. Commun. **11**, 5631 (2020).

[89] D. Opherden, M. S. J. Tepaske, F. Bärtl, M. Weber, M. M. Turnbull, T. Lancaster, S. J. Blundell, M. Baenitz, J. Wosnitza, C. P. Landee *et al.*, Field-Tunable Berezinskii-Kosterlitz-Thouless correlations in a Heisenberg magnet, Phys. Rev. Lett. **130**, 086704 (2023).

[90] A. S. T. Pires, B. V. Costa, and R. A. Dias, Phase diagram of the antiferromagnetic XY model in two dimensions in a magnetic field, Phys. Rev. B **78**, 212408 (2008).

[91] L. Hao, D. Meyers, H. Suwa, J. Yang, C. Frederick, T. R. Dasa, G. Fabbris, L. Horak, D. Kriegner, Y. Choi *et al.*, Giant magnetic response of a two-dimensional antiferromagnet, Nat. Phys. **14**, 806 (2018).

[92] S. Zhang, X. Li, H. Zhang, P. Cui, X. Xu, and Z. Zhang, Giant Dzyaloshinskii-Moriya interaction, strong XXZ-type biquadratic coupling, and bimeronic excitations in the two-dimensional $CrMnI_6$ magnet, npj Quantum Mater. **8**, 38 (2023).